IEEE Access
Multidisciplinary ⋮ Rapid Review ⋮ Open Access Journal

Received October 7, 2020, accepted October 11, 2020, date of publication October 14, 2020, date of current version October 27, 2020.

Digital Object Identifier 10.1109/ACCESS.2020.3031022

Reliability Evaluation of Multi-Mechanism Failure for Semiconductor Devices Using Physics-of-Failure Technique and Maximum Entropy Principle

BO WAN[1], (Member, IEEE), YE WANG[1], YUTAI SU[1,2], AND GUICUI FU[1], (Member, IEEE)
[1]School of Reliability and Systems Engineering, Beihang University, Beijing 100191, China
[2]Wolfson School of Mechanical, Electrical and Manufacturing Engineering, Loughborough University, Loughborough LE11 3TU, U.K.

Corresponding author: Yutai Su (suyutai@buaa.edu.cn)

This work was supported in part by the China Scholarship Council (CSC) under Grant 201906020125.

ABSTRACT The physics-of-failure (PoF) technique is a practical approach to evaluate the reliability of semiconductor devices. However, the PoF approaches are usually insufficient in dealing with multi-mechanism failure and fitting the Monte Carlo (MC) sampling data. In our study, we propose an improved reliability evaluation method based on PoF technique and maximum entropy (MaxEnt) principle. The PoF models are used to generate time-to-failure samples of the failure mechanisms. Cumulative damage rules and competing failure rules are adopted to deal with multi-point and multi-mechanism failure and generate lifetime samples of the device. And the lifetime samples are fitted by MaxEnt distributions through the proposed fitting algorithm. The numerical examples given in the paper indicate that the MaxEnt distributions can describe the samples well and have a competitive advantage in dealing with multi-peak samples. A case study about a semiconductor device with multi-mechanism failure is presented to explain the workflow of the proposed reliability evaluation approach. The results show that the proposed MaxEnt distributions can yield reliable reliability evaluation results compared with Weibull and Lognormal distributions in the multi-mechanism failure process.

INDEX TERMS Maximum entropy principle, multi-mechanism failure, physics-of-failure, semiconductor device reliability.

I. INTRODUCTION

The recent years have seen the rapid development of semiconductor devices in many fields such as 5G, Internet of things, artificial intelligence, etc. Owing to the increase of integration density and functional variety, reliable semiconductor devices play an increasingly important role in the electronic products or systems. Consequently, the reliability evaluation of semiconductor devices has aroused wide attention from both industry and academia. Reliability evaluations for semiconductor devices mostly have three kinds of approaches: empirical methods, testing methods and physics-of-failure (PoF) methods [1]. Among these, PoF methods are recognized as physics-based approaches that consider failure mechanisms and processes to predict the lifetime of semiconductor devices on their service conditions [2]. The notable advantage of using PoF methods is that it could describe potential failure mechanisms and evaluate the reliability during the design stage, so it could save the cost and time and is widely used in reliability prediction.

A considerable amount of literature on the reliability of semiconductor devices focuses mainly on various failure mechanisms. Kim *et al.* proposed a Spatio-temporal defect process model to evaluate the reliability of ultra-thin gate oxides breakdown for metal-oxide-semiconductor field effect transistor (MOSFET) [3]. Fu *et al.* implemented the failure models for the front end of line (FEoL), back end of line (BEoL) and Packaging failure mechanisms and competing failure rules to predict the reliability of system-in-package based on PoF methods [4]. Ahn *et al.* established a predictive model for integrated circuits (ICs). They implemented it to evaluate the IC reliability of FEOL and BEOL failure

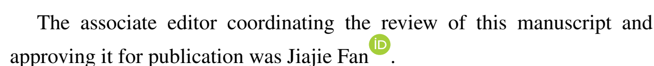
The associate editor coordinating the review of this manuscript and approving it for publication was Jiajie Fan.

This work is licensed under a Creative Commons Attribution 4.0 License. For more information, see https://creativecommons.org/licenses/by/4.0/

mechanisms, such as negative-bias temperature instability (NBTI), hot carrier injection (HCI), time-dependent breakdown (TDDB) and electromigration (EM) [5]. For packaging failure such as the fatigue of solder joint, the damage caused by thermal cycling and vibration can be regarded as a cumulative form. Qi *et al.* estimated lifetime of PBGA solder joints under combined loading conditions based on Engelmaier model and generalized Manson-Coffin model, and experiments were conducted to validate their estimation [6]. Eckert *et al.* compared the lifetime predicted by linear and incremental damage superposition approaches with the experimental results. They suggested a linear damage superposition approach to predict the lifetime of combined load cases [7]. Overall, PoF methods are practical in evaluating the reliability of semiconductor devices, but they do not go into details about the multi-mechanism failure process.

Monte-Carlo (MC) sampling, considering process variations and environmental fluctuations, has been employed to obtain the reliability results based on PoF methods. However, what remains unclear is how to select the appropriate distributions and fit the sampling data [8]. Xu *et al.* evaluated the modular multilevel converter (MMC) reliability utilizing MC simulations and obtained the Weibull lifetime distribution without being tested [9]. Jiao *et al.* fitted the three-parameter Weibull distribution of MC sampling data, which also showed poor fitting [10]. Qiu *et al.* performed the MC random sampling of HCI, NBTI and EM lifetime. They conducted the Kolmogorov-Smirnov test for lognormal distributions, Weibull distributions and normal distributions separately, and found the highest significance level of lognormal distributions for HCI, NBTI and EM failure lifetime [11]. Nevertheless, previous studies have failed to find a general distribution to fit the MC sampling data well in PoF methods.

There are considerable common reliability probability distributions, such as exponential, Weibull, normal and lognormal distributions [12]. Among these distributions, a maximum entropy (MaxEnt) probability distribution has the largest value of entropy and the least biased estimate on the given information [13]. Many researchers have attempted to fit the MaxEnt probability distribution function (PDF) from various sampling data based on the MaxEnt principle [14]–[17]. Zhang *et al.* approximated the structural performance function. They derived the reliability-based sensitivity index based on the principle of MaxEnt with fractional moment (FM), which determined accurate estimation results from MC simulations [18]. Xiong *et al.* established the Halphen distributions for the flood frequency analysis and used the MC simulation samples of the peak flows to obtain the 2-order MaxEnt, normal, exponential, Weibull, gamma, Pearson Type III (P3), generalized extreme value (GEV), and log-Pearson type III (LP3) distributions. P-values of Kolmogorov-Smirnov test, root-mean-square errors (RMSE) values and Akaike information criterion (AIC) values were calculated to prove the 2-order MaxEnt made better agreements than other distributions [19]. Arvind Rajan *et al.* exploited the high-order moments and developed a MaxEnt distribution fitting algorithm for the uncertainty evaluation. The 4-order MaxEnt, 8-order MaxEnt and Pearson distributions were conducted to fit the bimodal distribution, and the MaxEnt distributions showed a visible two peak pattern [20]. Taken together, the evidence reviewed here seems to suggest that the high-order MaxEnt distribution is an appropriate alternative to describe the MC sampling reliability data.

Based on the above research, it can be concluded that the existing PoF methods partially solve the reliability evaluation of semiconductor devices with MC simulations. However, more efforts are still needed, especially for the treatment of multi-mechanism failure and the fitting of the MC sampling data. In this paper, an improved reliability evaluation approach for semiconductor devices based on PoF technique and the MaxEnt principle is proposed. The PoF models, cumulative damage rules and competing failure rules are used to deal with the multi-mechanism failure process and can improve the accuracy of the lifetime sampling data. The MaxEnt distributions, derived from the MaxEnt principle, are used to fit the lifetime sampling data. The MaxEnt distributions can describe the sampling data well because the shape is flexible with the changeable order. And a case study is given to explain the workflow of the proposed reliability evaluation approach.

The remaining part of the paper proceeds as follows. Section 2 summarized the procedure of PoF method and introduced some typical PoF models and rules of the multi-mechanism failure process. In Section 3, the general form of MaxEnt PDF was derived from the MaxEnt principle, and the MaxEnt PDF fitting algorithm was formulated. Three numerical examples were applied in Section 4 to validate the accuracy of MaxEnt PDFs. A case study was presented in Section 5 to illustrate the reliability evaluation procedure and verify the effectiveness of this approach. The discussion was made in Section 6, and conclusions were summarized in Section 7.

II. PoF METHOD AND SAMPLING DATA ACQUISITION

PoF method is an approach to the design and assessment of reliable devices. The fundamental tools of PoF method are failure mechanism models, which are used to predict time-to-failure (TTF) corresponding to failure mechanisms. The failure mechanism model is a mathematical model that describes TTF as a function of loading conditions and parameters related to the manufacturing process. Equation (1) is a failure model of TDDB mechanism.

$$TTF = A_t \exp(-a_t E_{ox}/kT) \exp(E_{at}/kT) \tag{1}$$

where A_t is a parameter dependent on material and process detail, a_t is the effective dipole moment for the molecule (constant), E_{ox} is the externally applied electric field across the dielectric, E_{at} is the activation energy (constant), k is Boltzmann's constant, T is the local temperature.

The parameters in failure mechanism models are classified into stress-related parameter $\boldsymbol{S}$ and process-related parameter $\boldsymbol{\Theta}$. Stress-related parameter $\boldsymbol{S}$ is a set of parameters related

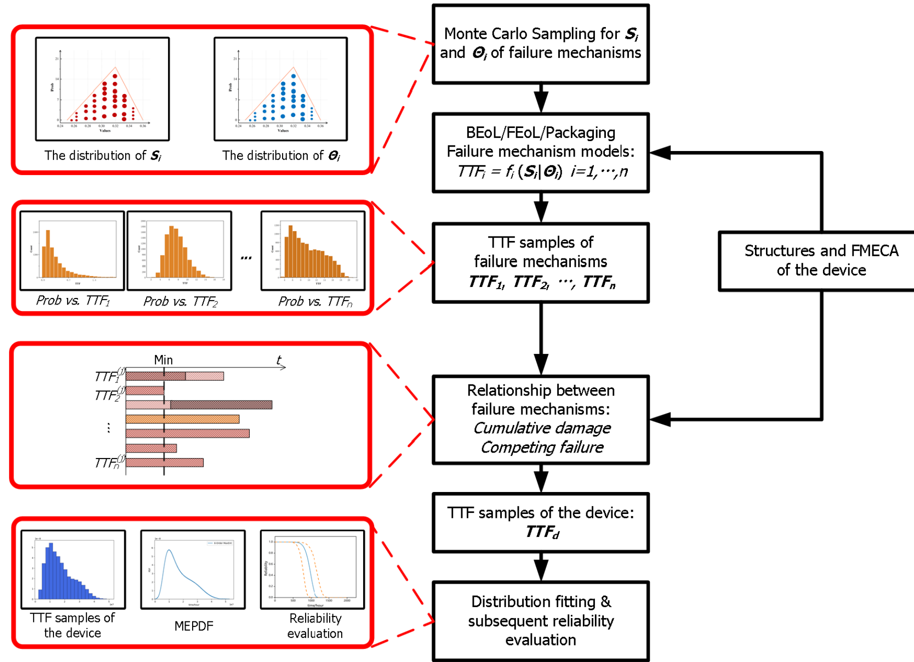

FIGURE 1. **The procedure of PoF method to evaluate the reliability of semiconductor devices considering cumulative damage and competing failure.**

to loading conditions (e.g., E_{ox} and temperature T in (1)); process-related parameter $\boldsymbol{\Theta}$ is process and materials related parameter set (e.g., A_t in (1)).

Due to the fluctuation of loading conditions and the instability of the manufacturing processes, parameters in $\boldsymbol{S}$ and $\boldsymbol{\Theta}$ are actually random variables and can be described by empirical random distribution like uniform, triangular or normal distribution.

The procedure of PoF method to evaluate reliability is shown in FIGURE 1. The samples of parameters $\boldsymbol{S}$ and $\boldsymbol{\Theta}$ are acquired first by Monte Carlo sampling from their distributions. Then, the parameter samples are used to calculate TTF and generate TTF samples s corresponding to failure mechanisms, using failure mechanism models. By considering the relationship between failure mechanisms, the TTF samples of the device can be obtained. The final reliability evaluation is conducted based on the lifetime distribution fitting of TTF samples.

A. PoF MODELS FOR TYPICAL FAILURE MECHANISMS

Failure mechanism refers to the specific physical or chemical process leading to the failure of devices. The TTF corresponding to the failure mechanism can be figured out by the failure mechanism model. The extensive researches on FEoL, BEoL and packaging failure mechanisms are conducted, and the failure mechanism models, including TDDB, HCI, EM, thermal fatigue *et al.*, are established. Common mature failure mechanism models are given in the TABLE 1. Those models are broadly applied in reliability evaluation and accelerated test design.

As shown in TABLE 1, most failure mechanism models take the form of Arrhenius model or Eyring model, e.g.,

TABLE 1. **Physics of failure mechanisms, models and positions in semiconductor devices.**

Failure mechanism	Failure mechanism models*	Failure positions	Ref.
TDDB	$TTF = A_t \exp(-a_t E_{ox}/kT)\exp(E_{at}/kT)$ a_t is the effective dipole moment for the molecule; E_{ox} is the externally applied electric field across the dielectric.	Gate oxide	[21-23]
HCI	$TTF = A_h (I_{sub})^{-N_h} \exp(E_{ah}/kT)$ I_{sub} is the peak substrate current during stressing; N_h is the exponent for I_{sub}.	Gate oxide	[24]
EM	$TTF = A_e (J - J_{crit})^{-N_e} \exp(E_{ae}/kT)$ J is the applied current density; J_{crit} is the critical current density of electro-migration; N_e is the exponent.	Metal trace	[25]
Stress Migration	$TTF = A_s (T_0 - T)^{-N_s} \exp(E_{as}/kT)$ T_0 is the stress-free temperature; N_s is the exponent.	Metal trace	[26, 27]
Corrosion	$TTF = A_c \exp(-a_c RH)\exp(E_{ac}/kT)$ a_c is the reciprocal humidity dependence parameter; RH is the relative humidity.	Metallization	[28]
Thermal fatigue	$N_f = K_1(\Delta W)^{K_2} + \dfrac{a_{tf}}{K_3(\Delta W)^{K_4}}$ N_f is the number of thermal cycles to failure.	Wire Bond, Solder layer	[29]
Vibration fatigue	$D = \dfrac{n_1}{N_1} + \dfrac{n_2}{N_2} + \dfrac{n_3}{N_3}$ D is the cumulative damage. While D equal to 1, the component failures.	Solder joint, packaging	[30]

*A is arbitrary constant, dependent on material and process detail, E_{a*} is the activation energy, k is Boltzmann's constant, T is temperature.

TDDB, HCI. But the thermal fatigue model and the vibration fatigue model have different forms. The thermal fatigue models of solder joint have many different forms. This paper presents a strain energy-based crack propagation model that is commonly used in the industry:

$$N_f = K_1(\Delta W)^{K_2} + \frac{a_{tf}}{K_3(\Delta W)^{K_4}} \tag{2}$$

where N_f is the number of thermal cycles to failure. ΔW is the increment of strain energy density per thermal cycle. a_{tf} is

the length of the solder joint. K_1, K_2, K_3, K_4 are arbitrary constant, which are dependent on materials.

The vibration fatigue model is derived from Steinberg's three-band method based on Gaussian distribution and Miner's linear cumulative damage law [30]:

$$D = \frac{n_1}{N_1} + \frac{n_2}{N_2} + \frac{n_3}{N_3}$$
$$N_i = \left(\frac{\Delta\varepsilon_i E}{3.5\sigma_u}\right)^n \quad (i = 1, 2, 3) \tag{3}$$

where n_i is the cumulative cycles corresponding to $i{*}\sigma$ strain range. $n_1 = 0.683N_0t$, $n_2 = 0.271N_0t$, $n_3 = 0.0433N_0t$. N_0 depends on the natural frequency of the device. N_i is the number of thermal cycles to failure of $i{*}\sigma$ strain range; t is the duration of vibration. $\Delta\varepsilon_i$ is the $i * \sigma$ strain range during vibration. E is Young's modulus of solder; σ_u is the tensile strength of solder, n is the fatigue component depends on the material.

B. RULES OF MULTI-MECHANISM FAILURE PROCESS

The failure mechanisms of the semiconductor devices are multiple and parallel, among which the relativity is complicated. By the number of failure mechanisms, the failure process can be classified into single-mechanism failure and multi-mechanism failure. Further, the multi-mechanism failure process can be divided into single-point failure and multi-point failure in accordance with the potential failure sites.

For semiconductor devices, the complicated failure process shows the characteristics of both multi-point failure and multi-mechanism failure. Reasonable cumulative damage rules can be utilized to describe the related failure mechanisms at each single failure point, and appropriate competing failure rules can be applied to analyze the unrelated failure mechanisms at each single failure point or between multiple points. Combining the cumulative damage rules and competing failure rules, the lifetimes of devices with a multi-mechanism failure process can be calculated.

1) COMPETING FAILURE RULES

Competing failure rules deal with unrelated failure mechanisms at a single point or multiple points. For single point failure, the failure is assumed to occur due to k competing failure mechanisms, and the corresponding calculated TTFs are, $TTF_{p,1}, TTF_{p,2}, \ldots, TTF_{p,k}$. In competing failure context, the lifetime of the specific point depends on the shortest of $TTF_{p,i}$, $i = 1, \ldots, k$. That is

$$TTF_p = \min\left(TTF_{p,1}, TTF_{p,2}, \ldots, TTF_{p,k}\right) \tag{4}$$

where TTF_p is the lifetime of single point.

For example, EM on the chip is activated by high current density and the failure mode is the cavity growth. HCI on the chip is caused by the strong electric field and the failure mode is threshold voltage shift, etc. There is little interaction between them, so the TTF of them can be calculated independently. It should be noted that there are still correlations between them. For example, the stress conditions are related: the power supply is single for the device, the electrical stress is related; the temperature across the transistor is almost the same, so the temperature for models of TDDB, HCI, EM should be the same; for the package, the humidity, temperature and vibration are also the same.

For multiple points, the lifetime of each point is calculated first. Failures occur at different points are assumed to be independent and failure at any point will lead to device failure. If there are m potential failure points in the device, the TTF of each point (TTF_{p1}, TTF_{p2}, …, TTF_{pm}) is calculated first. Then, by applying competing failure rules, the lifetime of the whole device TTF_D can be calculated by

$$TTF_D = \min\left(TTF_{p1}, TTF_{p2}, \ldots, TTF_{pn}\right) \tag{5}$$

2) CUMULATIVE DAMAGE RULES

The cumulative damage rules deal with related failure mechanisms at a single point. And series of cumulative damage theories can be employed in calculating the damage or predicting the lifetime of the specific point, such as Minner linear cumulative damage law, Marco-Starkey theory, Two-Stage linear damage theories.

For semiconductor devices, the cumulative damage rules are commonly used to describe damage accumulated by thermal fatigue and vibration fatigue [31]. Solder joint fatigue is a critical issue in the failure of device package. Under the service condition, thermal stress caused by CTE mismatching and mechanical stress induced by vibration damage the solder joint simultaneously. And both mechanisms contribute to solder deformation and crack propagation. Minner linear cumulative damage rule is adopted here to calculate the lifetime of solder joint. While thermal cycling and vibration are imposed to solder joint simultaneously, the accumulated damage per thermal cycle, D, has the form

$$D = \frac{f_v/f_t}{N_v} + \frac{1}{N_t} \tag{6}$$

where f_v is the natural frequency of the device, f_t is the frequency of thermal cycling; N_v and N_t are the predicted cycles to failure under single vibration and single thermal condition, respectively. Consequently, the lifetime of solder joint TTF_R can be calculated

$$TTF_R = \frac{1}{D} \times T_t = \frac{N_v \cdot N_t}{f_t \cdot N_v + f_v \cdot N_t} \tag{7}$$

where T_t is the period of thermal cycling. Let $TTF_v = N_v/f_v$, and $TTF_t = N_t/f_t$, then

$$TTF_R = \frac{TTF_v \cdot TTF_t}{TTF_v + TTF_t} \tag{8}$$

It should be noted that there may be more complicated interactions between failure mechanisms, e.g., narrowing of metal trace induced by EM or SM will change the current and voltage stress of TDDB and HCI. These complicated interactions are not considered in this paper because there

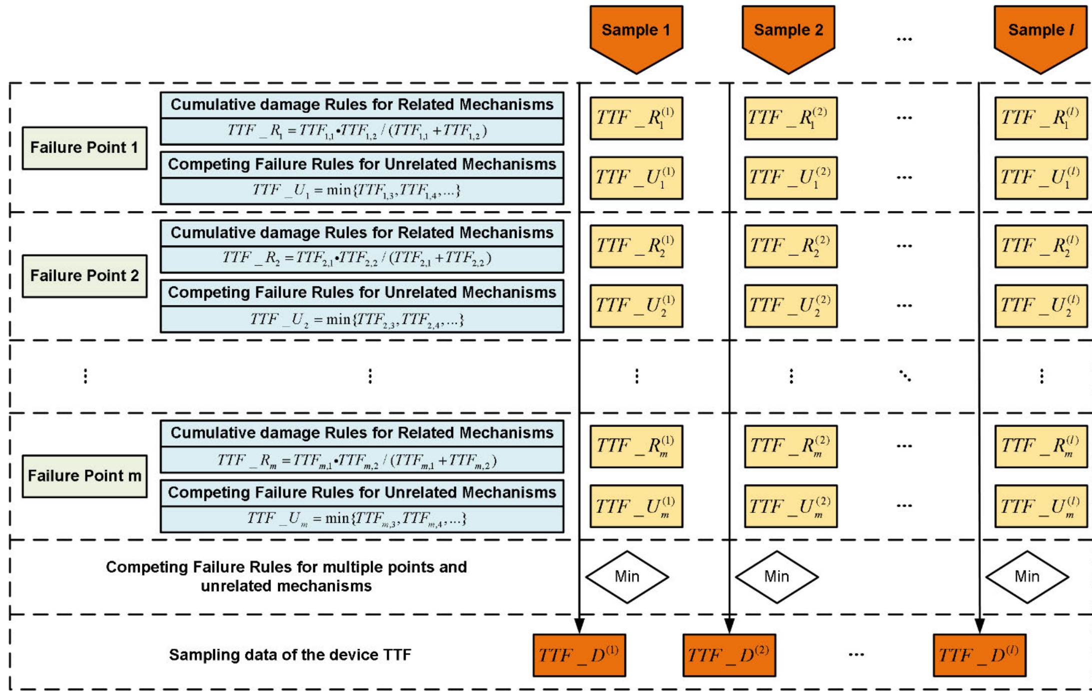

FIGURE 2. The flowchart of Monte Carlo sampling method for multi-mechanism failure.

are no broadly accepted theories for them, and they are complex issues that require in-depth research. This paper mainly focuses on the PoF procedure and the MaxEnt principle, so a simple and practical method is adopted for the treatment of multi-mechanism failures. The whole procedure of the paper can still be applied if the interactions are further studied and considered.

C. MC SAMPLING FOR MULTI-MECHANISM FAILURE DATA

Monte Carlo sampling is applied in our study to provide a mass of lifetime samples of the device for the subsequent distribution fitting. MC sampling generates reliable sampling data, considering the stochastic parameters and complex multi-mechanism failure processn. The MC method can be explained by FIGURE 2.

First, TTF sampling data for each potential mechanism at each failure point are acquired by PoF models and stochastic parameter sampling. $TTF_{i,j}^{(k)}$ is the kth calculated TTF of jth mechanism at ith point, $i = 1, 2, \ldots, m$, $j = 1, 2, \ldots, n_i$, $k = 1, 2, \ldots, l$, where m is the number of potential failure points, n_i is the number of involved mechanisms at ith point, l is the number of samples. Then, TTF of related mechanisms can be calculated by applying cumulative damage rules:

$$TTF_R_i^{(k)} = TTF_{i,1}^{(k)} \cdot TTF_{i,2}^{(k)} / \left(TTF_{i,1}^{(k)} + TTF_{i,2}^{(k)} \right) \quad (9)$$

where $TTF_{i,j}^{(k)}$ represents kth TTF sample due to related mechanisms at ith point.

And TTF for single-point unrelated mechanisms is obtained according to competing failure rules:

$$TTF_U_i^{(k)} = \min \left\{ TTF_{i,3}^{(k)}, TTF_{i,4}^{(k)}, \ldots TTF_{i,n_i}^{(k)} \right\} \quad (10)$$

where $TTF_U_i^{(k)}$ represents kth TTF sample due to unrelated mechanisms at ith point.

Finally, l lifetime sampling data of the device $TTF_D^{(1)}$, $TTF_D^{(2)}, \ldots, TTF_D^{(l)}$ can be obtained by applying competing failure rules to multiple points and unrelated mechanisms. The sampling data acquired by MC sampling procedure can be used to fit the lifetime distribution of the device.

III. MaxEnt FITTING OF SAMPLING DATA

The MaxEnt PDF derived from the MaxEnt principle is presented in this section. A fitting algorithm with MLE and integral interval transformation was proposed to solve the MaxEnt PDF. The sampling data generated by Section II will be fitted by the MaxEnt PDF. Furthermore, the fitted MaxEnt PDF will be be used to evaluate reliability.

The 3-order to 7-order MaxEnt PDFs were fitted in the paper. Because the 1-order and 2-order MaxEnt PDFs are in forms of exponential and normal PDFs, which cannot reflect the specialty of MaxEnt PDFs. In general, we are inclined to use higher order MaxEnt PDFs because they have higher degrees of freedom, which means they can better describe objective data and thus can make a more accurate reliability evaluation. However, fitting higher order consumes more computing resources and time and improves the fitting limitedly. Hence, the order is limited to seven in our study.

Meanwhile, the 3-order to 7-order MaxEnt PDFs are broadly used in relevant research.

A. MaxEnt PRINCIPLE

The concept of information-theory entropy was proposed by Shannon [32] to describe the amount of uncertainty, expressed as:

$$H(p) = -\sum_{k=1}^{n} p_k \ln p_k \tag{11}$$

where $p_1, p_2, \ldots, p_n$ are probabilities of random events, and there are two constraints: $p_k > 0$ and $\Sigma p_k = 1$. For a continuous random variable X, with the density function $f(x)$, the entropy function can be given as

$$H[f(x)] = -\int_{-\infty}^{+\infty} f(x)[\ln f(x)]dx \tag{12}$$

In terms of the MaxEnt principle [13], the PDFs with the maximum entropy can best describe the existing knowledge. Supposing that the first few origin moments of an arbitrary random variable are known, the MaxEnt PDF that gives the smallest estimation error can be optimized and obtained as follows:

$$\text{Maximize: } H[f(x)] = -\int_{-\infty}^{+\infty} f(x)[\ln f(x)]dx \tag{13}$$

$$\text{Subjected to: } \int_{-\infty}^{+\infty} f(x)dx = 1 \tag{14}$$

$$\int_{-\infty}^{+\infty} x^i f(x)dx = m_i, \quad i=0,1,\ldots,n \tag{15}$$

where $f(x)$ is the PDF of a random variable X and m_i is the ith-order origin moment as the constraint, which can be determined by the random variable X.

The Lagrange method is used to work out the MaxEnt PDF from (13), (14) and (15). The Lagrangian function $L(x)$ is established with the moment constraints,

$$L(x) = H[f(x)] + \lambda_0 \left[\int_{-\infty}^{+\infty} f(x)dx - 1\right] + \sum_{i=1}^{n} \lambda_i \left[\int_{-\infty}^{+\infty} x^i f(x)dx - m_i\right] \tag{16}$$

where λ_i $(i = 0, 1, \ldots, n)$ is the unknown Lagrange multiplier.

According to moment constraints, the maximum of the Lagrangian function can be solved as follow:

$$\frac{\partial L(x)}{\partial f(x)} = -\int_{-\infty}^{+\infty} \{\ln[f(x)] + 1\}dx + \lambda_0 \int_{-\infty}^{+\infty} 1dx + \sum_{i=1}^{n} \lambda_i \left(\int_{-\infty}^{+\infty} x^i dx\right) = 0 \tag{17}$$

$$\int_{-\infty}^{+\infty} \left\{-\ln[f(x)] - 1 + \lambda_0 + \sum_{i=1}^{n} \lambda_i x^i\right\} dx = 0 \tag{18}$$

$$-\ln[f(x)] - 1 + \lambda_0 + \sum_{i=1}^{n} \lambda_i x^i = 0 \tag{19}$$

$$\ln[f(x)] = -1 + \lambda_0 + \sum_{i=1}^{n} \lambda_i x^i \tag{20}$$

Then, the MaxEnt PDF is expressed as:

$$f(x) = \exp\left(-1 + \lambda_0 + \sum_{i=1}^{n} \lambda_i x^i\right) \tag{21}$$

Referring to (14), the Lagrange multiplier, λ_0, is derived as:

$$\lambda_0 = 1 + \ln \int_{-\infty}^{+\infty} \exp\left(\sum_{i=1}^{n} \lambda_i x^i\right) dx \tag{22}$$

B. MaxEnt PDF FITTING ALGORITHM

A fitting algorithm with MLE method and integral interval transformation is proposed to obtain the 1-order to M-order MaxEnt PDFs. MLE method is used to reduce the computing difficulty and improve the algorithm efficiency. Meanwhile, the integral interval transformation can prevent computation overflow. With these above methods, the flowchart of the MaxEnt PDF fitting algorithm is shown in FIGURE 3.

The procedure to fit the 1-order to M-order MaxEnt PDFs consists of eight basic steps, as follows.

Algorithm 1 MaxEnt PDF fitting algorithm

Step 1: Generate the random samples $x_1, x_2, \ldots, x_l$ using MC sampling based on PoF method.

Step 2: Transform the random samples $x_1, x_2, \ldots, x_l$ to $x'_1, x'_2, \ldots, x'_l$ using (32) by integral interval transformation method.

Step 3: Calculate the origin moments m'_i $(i = 1, 2, \ldots, M)$ of the transformed random samples $x'_1, x'_2, \ldots, x'_l$, and set the iteration counter $n = 0$.

Step 4: Set n = n+1, and set the initial values λ' $[\lambda'_1, \lambda'_2, \ldots, \lambda'_{n-1}, 0]$ of the Lagrange multipliers, then solve the optimization problem shown as (26) and (27) using the nonlinear optimization method (e.g., downhill simplex method, Quasi-Newton Method, etc.).

Step 5: Get the n-order Lagrange multipliers λ' $[\lambda'_0, \lambda'_1, \lambda'_2, \ldots, \lambda'_n]$, and save them to the database.

Step 6: Judge whether $n = M - 1$. if Yes, go to step 7; if no, go to step 4.

Step 7: Read the 1-order to M-order Lagrange multipliers λ' from the database, and transform all Lagrange multipliers λ' to λ.

Step 8: Determine the 1-order to M-order MaxEnt PDFs.

In this algorithm, the random samples $x_1, x_2, \ldots, x_l$ are lifetime samples $TTF_D^{(1)}$, $TTF_D^{(2)}$, …, $TTF_D^{(l)}$ of the device, acquired by MC sampling procedure in Section II. In the algorithm, a sequential update strategy was adopted,

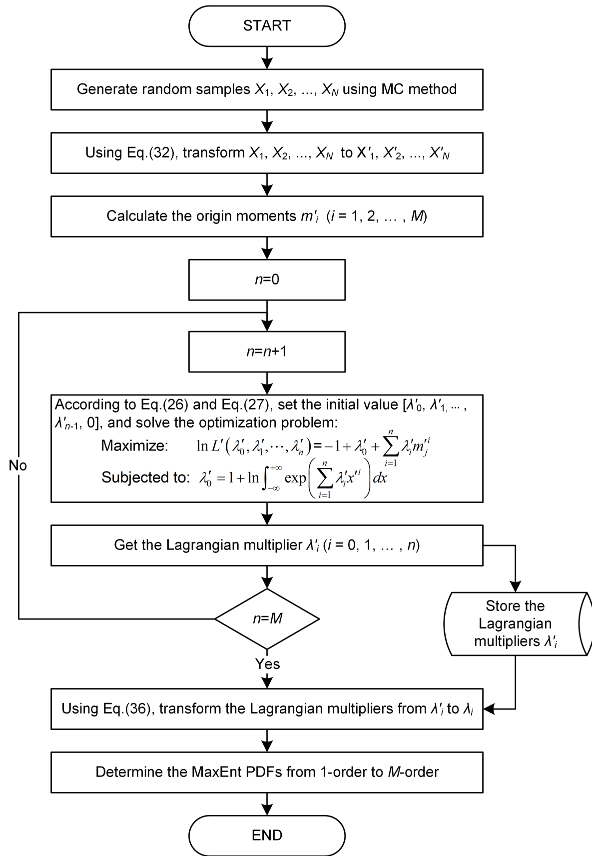

FIGURE 3. The flowchart of MaxEnt PDF fitting algorithm.

which can obtain 1-order to M-order MaxEnt PDFs. Meanwhile, due to the set of initial values from previous results, the algorithm has not only the computational efficiency but also the enhanced accuracy. For the nonlinear optimization algorithm, the downhill simplex method was chosen because of the fast computing speed. This algorithm in the study fitted the 3-order to 7-order MaxEnt PDFs. However, the 1-order and 2-order MaxEnt PDFs with little significance were ignored, considering that they are other forms of exponential and normal PDFs.

1) MAXIMUM-LIKELIHOOD ESTIMATION

In this paper, we use the MLE method to obtain the parametric estimated value of the MaxEnt PDF.

Suppose $x_1, x_2, \ldots, x_l$ is a continuous random sample and X subjects to the MaxEnt probability distribution. Under this case, the likelihood function of MaxEnt PDF is given by

$$L(\lambda_0, \lambda_1, \cdots, \lambda_n) = \prod_{j=1}^{l} \exp\left(-1 + \lambda_0 + \sum_{i=1}^{n} \lambda_i x_j^i\right) \quad (23)$$

In order to avoid the excessive value of the likelihood function, the modified likelihood function L' with a modified exponent $1/l$ is given by

$$L'(\lambda_0, \lambda_1, \cdots, \lambda_n) = \left[\prod_{j=1}^{l} \exp\left(-1 + \lambda_0 + \sum_{i=1}^{n} \lambda_i x_j^i\right)\right]^{\frac{1}{l}} \quad (24)$$

The logarithm of the modified likelihood function (24) is given by

$$\begin{aligned} \ln L'(\lambda_0, \lambda_1, \cdots, \lambda_n) &= \frac{1}{l} \sum_{j=1}^{l} \left(-1 + \lambda_0 + \sum_{i=1}^{n} \lambda_i x_j^i\right) \\ &= -1 + \lambda_0 + \sum_{i=1}^{n} \lambda_i \left(\frac{1}{l} \sum_{j=1}^{l} x_j^i\right) \\ &= -1 + \lambda_0 + \sum_{i=1}^{n} \lambda_i m_j^i \end{aligned} \quad (25)$$

where m_i is the ith-order origin moment. Based on the MLE method, let the Lagrange multiplier λ_i (i = 0, 1, …, n) be the optimization variables, the optimization problem can be determined as

$$\text{Maximize: } \ln L'(\lambda_0, \lambda_1, \cdots, \lambda_n) = -1 + \lambda_0 + \sum_{i=1}^{n} \lambda_i m_j^i \quad (26)$$

$$\text{Subjected to: } \lambda_0 = 1 + \ln \int_{-\infty}^{+\infty} \exp\left(\sum_{i=1}^{n} \lambda_i x^i\right) dx \quad (27)$$

As showed above, though the MaxEnt PDF has the characteristic of highly non-linearity, the MLE method is conducted to lower the non-linearity of MaxEnt PDF and reduce the difficulties of optimization solutions.

2) INTEGRAL INTERVAL TRANSFORMATION

In solving the Lagrange multiplier λ_i (i = 0, 1, …, n), the integral calculations of the exponential part are likely to overflow and fail due to the high lifetime value of the upper and lower boundaries. Transformation of integration interval can be used to prevent the excessive numerical values of the Lagrange multiplier. The transformation algorithm transforms the initial interval to a proper target interval, which has a small interval upper and lower bounds and is accessible to calculation.

Suppose the initial interval of a MaxEnt PDF $f(x)$ is $l \le x \le u$, shown as (28), the target interval is $l' \le x' \le u'$, and the transformed MaxEnt PDF $f'(x')$ is given by (29).

$$f(x) = \exp\left(-1 + \lambda_0 + \sum_{i=1}^{n} \lambda_i x^i\right), \quad l \le x \le u \quad (28)$$

$$f'(x') = \exp\left(-1 + \lambda'_0 + \sum_{i=1}^{n} \lambda'_i x'^i\right), \quad l' \le x' \le u' \quad (29)$$

For the convenience of calculation, constant S and A are introduced, defined as

$$S = \frac{u' - l'}{u - l} \tag{30}$$

$$A = \frac{Sl - l'}{S} \tag{31}$$

Using S and A, the relationship of x and x' is given by (32), and the relationship of $f(x)$ and $f'(x')$ is given by (33).

$$x = A + \frac{x'}{S} \tag{32}$$

$$f(x) = Sf'\left(x'\right) \tag{33}$$

Substituting (32) and (33) into (29), we have

$$\frac{1}{S}f(x) = \exp\left\{-1 + \lambda_0' + \sum_{i=1}^{n} \lambda_i'[S(x-A)]^i\right\}, \tag{34}$$

that is,

$$f(x) = \exp[-1 + \ln S + \lambda_0' + \sum_{i=1}^{n} \lambda_i' S^i (-A)^i - \sum_{i=1}^{n} \lambda_i' S^i \sum_{j=1}^{i} C_i^j x^j (-A)^{i-j}] \tag{35}$$

where C_i^j is the number of j-combinations of an i-set.

From (32) and (35), the relationship of the Lagrange multiplier vector λ and the transformed Lagrange multiplier vector λ' can be given by

$$\lambda^T = G\lambda'^T \tag{36}$$

where the transforming matrix G is given by and the Lagrange multiplier vector λ and the transformed Lagrange multiplier vector λ' are given by

$$\lambda = \left[\ln S + \lambda_0 \ \lambda_1 \ \lambda_2 \ \cdots \ \lambda_{n-1} \ \lambda_n\right] \tag{38}$$

$$\lambda' = \left[\lambda_0' \ \lambda_1' \ \lambda_2' \ \cdots \ \lambda_{n-1}' \ \lambda_n'\right] \tag{39}$$

The transformation method of integration interval is an adjunct to the MaxEnt fitting algorithm, which converts the initial interval to a small interval [0,1], to avoid calculation overflow, save time and improve efficiency.

C. PERFORMANCE OF THE FITTING ALGORITHM

In order to examine the performance of the MaxEnt PDF fitting algorithm, the data sampled from Weibull distribution, Lognormal distribution, and Bimodal distribution were fitted. The Weibull distribution and Lognormal distribution are widely used in reliability evaluation. And Bimodal distribution is appropriate for describing the failure with two or more failure mechanisms.

As part of numerical analysis, two discrimination criteria, the root-mean-square error (RMSE) and the Akaike information criterion (AIC) were computed to evaluate the descriptive ability of the MaxEnt PDFs. RMSE can measure the goodness of data fits, and AIC can reward not only the accuracy of the fitted PDFs but also contains a penalty which is increased by the number of estimated parameters. The RMSE and AIC can be given by [33]:

$$\text{RMSE} = \sqrt{\frac{1}{n}\sum_{i=1}^{n}\left(\frac{\hat{y}_i - y_i}{y_i}\right)^2} \tag{40}$$

$$\text{AIC} = n \cdot \ln\left\{\frac{1}{n}\sum_{i=1}^{n}\left(\frac{\hat{y}_i - y_i}{y_i}\right)^2\right\} + 2K \tag{41}$$

where $\hat{y}_i$ is the estimate of y_i, y_i is the sample point in the histogram, and K is the number of parameters to be fitted.

1) EXAMPLE 1: WEIBULL DISTRIBUTION

In this subsection, three datasets from Weibull distribution are given by MC sampling, the sampling numbers of which are separately 10^3, 10^4 and 10^5. The parameters of Weibull distribution are the shape parameter $\beta = 1.50$, the scale parameter $\alpha = 2000$, the location parameter $\gamma = 10000$.

The estimations of three datasets, sampling number $N = 1000, 10000, 10000$, using Lognormal method, Weibull method and MaxEnt method with order numbers $n = 3$ to 7 are shown in FIGURE 4. Then, the values of RMSE and AIC, shown in TABLE 2, are calculated to evaluate both the goodness of fits and the simplicity of the model. Finally, the lifetime predictions, including average lifetime, medium lifetime and interval estimation ($CL = 95\%$), are conducted by the above three methods and compared with the sampling data, given by TABLE 3.

Based on FIGURE 4, the fitting curves of Weibull PDF and high-order ($n = 6, 7$) MaxEnt PDFs and reliability distributions match the sampling data better than these of Lognormal and low-order ($n = 3, 4$) MaxEnt PDF and reliability distributions.

More quantitive analysis can be carried out according to TABLE 2. The RMSEs and AICs of Weibull PDF and high-order MaxEnt PDFs are minimal, which means Weibull PDF and high-order MaxEnt PDFs achieve higher accuracy and efficiency for Weibull sampling data than Lognormal PDF. Further, the RMSEs of MaxEnt PDFs under the conditions of small sampling number (N = 1000, 10000) are less than these of Weibull PDF. Constantly, when $N = 100000$, Weibull PDF fits the sampling data better than MaxEnt PDFs. For the AICs, the Weibull PDF is more effective than high-order MaxEnt PDFs due to the fewer parameters. The average lifetime, medium lifetime and confidence interval (95%) are obtained by sampling data, Lognormal distribution, Weibull distribution and MaxEnt distributions ($n = 3$ to 7), shown in TABLE 3. Compared with the results of sampling data, Weibull distribution and high-order MaxEnt distributions predict more accurately than Lognormal distribution.

2) EXAMPLE 2: LOGNORMAL DISTRIBUTION

Lognormal MC sampling ($N = 10^3, 10^4, 10^5$) is conducted to obtain three datasets in this subsection, and the parameters of the Lognormal distributions are $\mu = 100000$, $\sigma^2 = 0.05$.

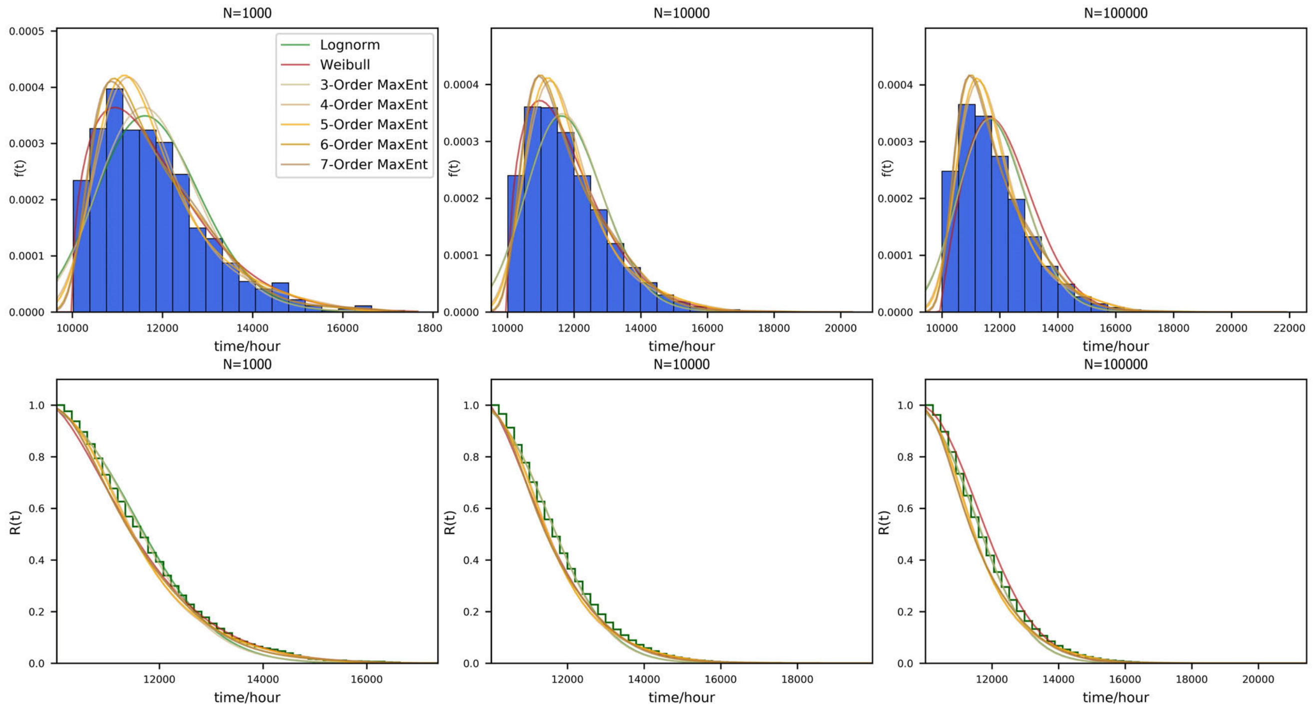

FIGURE 4. Estimated PDFs and reliability functions of Weibull MC sampling (N = 1000, N = 10000, N = 100000) using Lognorm method, Weibull method and MaxEnt method with order numbers n = 3 to 7.

TABLE 2. The RMSE and AIC of Lognorm method, Weibull method and MaxEnt method with order numbers n = 3 to 7 to fit the Weibull MC Sampling data (N = 1000, N = 10000, N = 100000).

		Lognormal distribution	Weibull distribution	MaxEnt distribution				
				3-order	4-order	5-order	6-order	7-order
$n = 10^3$	RMSE	0.010101327	0.010099655	0.010100982	0.010099631	0.010099501	0.010099334	**0.010099298**
	AIC	16983.56	**16810.70**	16972.49	16883.05	16865.8	16828.2	16824.44
$n = 10^4$	RMSE	0.003597547	0.003597077	0.003597539	0.003597053	0.003597018	0.003596991	**0.003596990**
	AIC	169846.20	**168132.8**	169902.1	168823.6	168657	168308.8	168253
$n = 10^5$	RMSE	0.001188679	**0.001188496**	0.001188685	0.001188528	0.001188520	0.001188515	0.001188514
	AIC	1696944	**1677978**	1698187	1686377	1684999	1682084	1681515

The parameters of Lognormal, Weibull and MaxEnt ($n = 3$ to 7) distributions are estimated to fit the three datasets of Lognormal MC sampling (N = 1000, 10000, 100000) and plotted in FIGURE 5. The RMSEs and AICs are computed in TABLE 4. Moreover, the results of lifetime predictions are shown in TABLE 5.

FIGURE 5 shows the approximation of the Lognormal MC sampling data by the Lognormal, Weibull, MaxEnt ($n = 3$ to 7) PDFs and reliability distributions. Weibull distribution has a more significant mismatch than other distributions from the qualitative perspective.

Considering the values of the RMSE and AIC, Lognormal and MaxEnt distributions have better goodness of fit than Weibull distribution, shown in TABLE 4. The RMSEs of low-order ($n = 3,4$) MaxEnt distribution are below Lognormal distribution. On the contrary, the AICs of Lognormal

$$G = \begin{bmatrix} C_0^0 S^0(-A)^0 & C_1^0 S^1(-A)^1 & \cdots & C_{n-1}^0 S^{n-1}(-A)^{n-1} & C_n^0 S^n(-A)^n \\ 0 & C_1^1 S^1(-A)^0 & \cdots & C_{n-1}^1 S^{n-1}(-A)^{n-2} & C_n^1 S^n(-A)^{n-1} \\ \vdots & \vdots & \ddots & \vdots & \vdots \\ 0 & 0 & \cdots & C_{n-1}^{n-1} S^{n-1}(-A)^0 & C_n^{n-1} S^n(-A)^1 \\ 0 & 0 & \cdots & 0 & C_n^n S^n(-A)^0 \end{bmatrix} \tag{37}$$

TABLE 3. Lifetime predictions (Hours) of Weibull MC sampling (N = 100000) by Lognormal method, Weibull method and MaxEnt method with order numbers n = 3 to 7.

	Sampling data	Lognormal distribution	Weibull distribution	MaxEnt distribution				
				3-order	4-order	5-order	6-order	7-order
Average	**11809.58**	11808.06	11809.24	11809.57	11755.47	11584.96	11566.26	**11809.58**
Medium	**11574.33**	11749.54	**11570.12**	11755.47	9621.23	10022.67	10059.84	11537.32
Interval estimation ($CL = 95\%$)	**(10172.26, 14786.79)**	(9664.40, 14284.56)	**(10173.22, 14782.00)**	(9621.23, 14267.12)	(14267.12, 11809.58)	(14973.54, 11809.58)	(14929.84, 11809.58)	(10152.75, 14685.18)

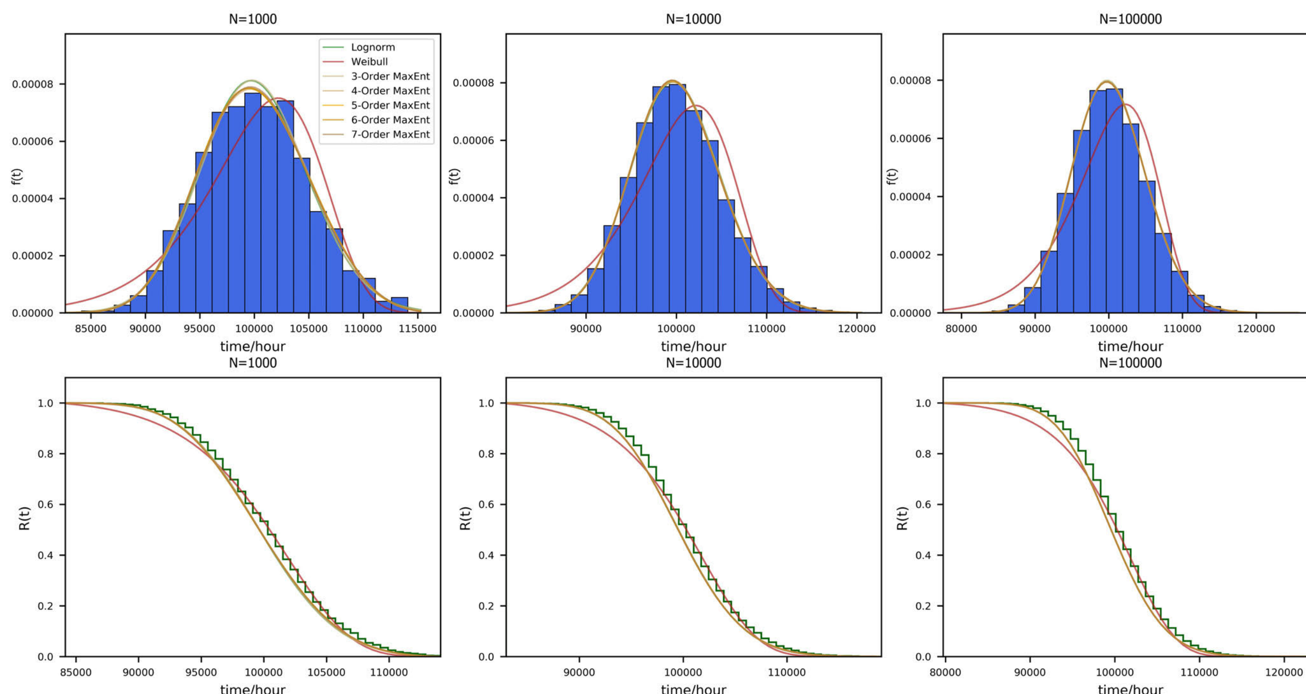

FIGURE 5. Estimated PDFs and reliability functions of Lognormal MC sampling (N = 1000, N = 10000, N = 100000) using Lognorm method, Weibull method and MaxEnt method with order numbers n=3 to 7.

TABLE 4. The RMSE and AIC of Lognorm method, Weibull method and MaxEnt method with order numbers n = 3 to 7 to fit the Lognormal MC sampling data (N = 1000, N = 10000, N = 100000).

		Lognormal distribution	Weibull distribution	MaxEnt distribution				
				3-order	4-order	5-order	6-order	7-order
$n = 10^3$	RMSE	0.009484255	0.009484774	**0.009484249**	0.009484267	0.009484262	0.009484260	0.009484260
	AIC	**19862.52**	20027.46	19866.65	19868.11	19869.85	19871.77	19873.77
$n = 10^4$	RMSE	0.003601024	0.003601156	0.003601023	**0.003601022**	0.003601023	0.003601023	0.003601023
	AIC	**198658.87**	200243.80	198661.12	198663.01	198664.49	198666.49	198667.42
$n = 10^5$	RMSE	0.0011923621	0.0011924036	**0.0011923617**	0.0011923621	0.0011923621	0.0011923621	0.0011923620
	AIC	**1987196.25**	2003499.70	1987203.73	1987202.03	1987203.99	1987205.99	1987206.63

distribution are lower than MaxEnt distribution. The order number of MaxEnt distribution has little influence on the accuracy of data fitting, so that increasing order number presents a higher value of AIC. For the lifetime prediction, TABLE 5 shows the Lognormal and MaxEnt distribution can predict the lifetime from sampling data more accurately than Weibull distribution.

3) EXAMPLE 3: BI-MODAL DISTRIBUTION

A complex bi-modal distribution, more accordant with multi-mechanism failure, is defined as a sum of two Gaussian distributions [34]. Assuming two main mechanisms of the device failure are subject to two independent normal distributions with different proportions, shown in TABLE 6, three datasets are generated by MC sampling ($N = 1000, 10000, 100000$).

TABLE 5. Lifetime predictions (Hours) of Lognormal MC sampling (N = 100000) by Lognormal method, Weibull method and MaxEnt method with order numbers n = 3 to 7.

	Sampling data	Lognormal distribution	Weibull distribution	MaxEnt distribution 3-order	4-order	5-order	6-order	7-order
Average	**100126.88**	100126.87	99815.13	**100126.88**	100002.44	99998.72	99998.00	100126.88
Medium	**100008.02**	100001.84	100670.68	**100002.44**	90659.11	90675.54	90676.04	99998.53
Interval estimation (*CL* = 95%)	**90672.03**	**90668.40**	85306.59	90659.11	110305.64	110305.05	110307.34	90666.52
	110371.61	110296.07	109451.72	110305.64	100126.88	100126.88	100126.88	**110318.41**

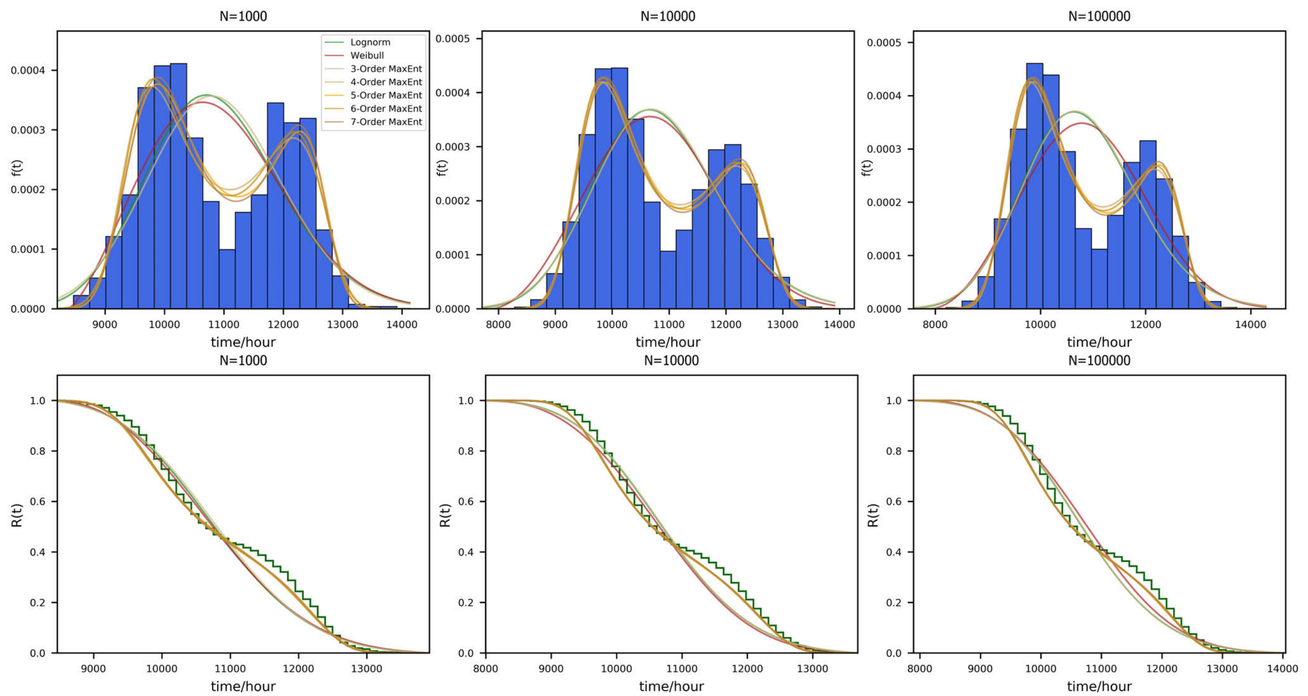

FIGURE 6. Estimated PDFs and reliability functions of bi-modal MC sampling (N = 1000, N = 10000, N = 100000) using Lognormal method, Weibull method and MaxEnt method with order numbers n = 3 to 7.

TABLE 6. The parameters for bi-modal MC sampling.

Distribution type	X_1 Distribution	Weight factor W_1	X_2 Distribution	Weight factor W_2
bi-modal distribution	$X_1 \sim$ Normal (0, 1)	0.6	$X_2 \sim$ Normal (0, 1)	0.4

Lognormal, Weibull, and MaxEnt ($n = 3$ to 7) distributions are fitted to the bi-modal MC sampling shown in FIGURE 6. The RMSEs and AICs are calculated in TABLE 7, and the lifetimes are predicted in TABLE 8 by Lognormal, Weibull, and MaxEnt method.

Lognormal, Weibull, and MaxEnt ($n = 3$ to 7) distributions are fitted to the bi-modal MC sampling shown in FIGURE 6. The RMSEs and AICs are calculated in TABLE 7, and the lifetimes are predicted in TABLE 8 by Lognormal, Weibull, and MaxEnt method.

FIGURE 6 presents that 4 to 7 order MaxEnt PDFs with obvious double peaks accord well with the bi-modal distribution. However, Lognormal, Weibull, and 3-order MaxEnt PDFs show single peaks which can not describe the bi-modal distribution well. For bi-modal MC sampling data (N = 1000, 10000, 10000), the fitting ability and predictive power of high order MaxEnt PDFs are better than the Lognormal and Weibull PDFs, according to RMSEs and AICs showed in TABLE 7. As to the prediction results of average lifetimes, medium lifetimes and interval estimations, the 7-order MaxEnt method agree best with the sampling data among all methods, shown in TABLE 8.

In conclusion, we compare the fitting prediction results for different sampling data by Weibull, Lognormal and MaxEnt methods. MaxEnt distribution exhibits an excellent agreement with the sampling distributions. Especially for bi-modal sampling, the 7-order MaxEnt distribution describes the feature of double peaks accurately and effectively.

IV. CASE STUDY

In this case, we evaluate the reliability of a typical plastic package device to demonstrate the PoF and MaxEnt based reliability evaluation method. The device is assembled

TABLE 7. The RMSE and AIC of Lognormal method, Weibull method and MaxEnt method with order numbers n = 3 to 7 to fit the bi-modal MC sampling data (N = 1000, N = 10000, N = 100000).

		Lognormal distribution	Weibull distribution	MaxEnt distribution				
				3-order	4-order	5-order	6-order	7-order
$n = 10^3$	RMSE	0.00881080	0.00881035	0.00881101	0.00880736	0.00880702	0.00880699	**0.00880671**
	AIC	16882.61	16837.06	16894.64	16637.46	16630.87	16625.78	**16620.45**
$n = 10^4$	RMSE	0.00287271	0.00287268	0.00287276	0.00287153	0.00287149	0.00287146	**0.00287142**
	AIC	168241.21	168078.26	168363.35	165630.36	165596.86	165546.62	**165512.92**
$n = 10^5$	RMSE	0.00095018	0.00095022	0.00095020	0.00094982	0.00094980	0.00094979	**0.00094978**
	AIC	1681551.47	1679404.43	1682757.03	1655137.27	1654597.65	1654231.14	**1653786.93**

TABLE 8. Lifetime predictions (Hours) of bi-modal MC sampling (N = 100000) by Lognormal method, Weibull method and MaxEnt method with order numbers n = 3 to 7.

	Sampling data	Lognormal distribution	Weibull distribution	MaxEnt distribution				
				3-order	4-order	5-order	6-order	7-order
Average	**10799.36**	10799.10	10862.16	10799.36	10750.86	10586.76	10568.14	**10799.36**
Medium	**10480.40**	10744.24	10831.89	10750.86	8783.72	9170.76	9150.38	**10560.02**
Interval estimation ($CL = 95\%$)	**(9133.94, 12758.98)**	(8815.84, 13094.46)	(8850.70, 13070.40)	(8783.72, 13095.02)	(13095.02, 10799.36)	(12780.52, 10799.36)	(12759.99, 10799.36)	**(9154.64, 12754.68)**

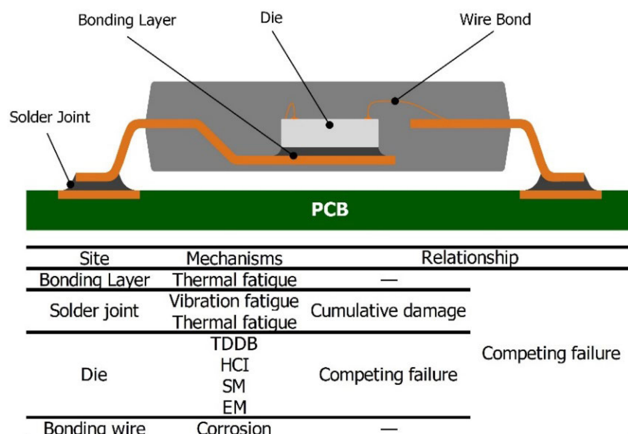

FIGURE 7. The structure of a typical semiconductor device with the potential multi-mechanism failure.

on the printed circuit board and is characterized by multi-mechanism. FIGURE 7 illustrates the structure of a typical semiconductor device with potential multi-mechanism failure. The electrical and mechanical connections between the die and the lead frame are made by bonding layer and bonding wire. The vulnerable sites involve the die, bonding wire, bonding layer and solder joint. The relationship between failure mechanisms is presented in FIGURE 7. The correlation of failure mechanisms is that they share the same stress and environmental conditions. For example, TDDB, HCI, EM, SM on the die have the same temperature.

TDDB, HCI, EM, and SM are recognized as the main mechanisms leading to die failure, and the relationship for them is competition. The *TTF* of the die is

$$TTF_{DE} = \min\left(TTF_{TDDB}, TTF_{HCI}, TTF_{EM}, TTF_{SM}\right). \quad (42)$$

Failure of solder joint is triggered by the accumulation of damage contributed by thermal cycling and vibration. The *TTF* of solder joint can therefore be determined

$$TTF_{SV} = T_c / D_{VF} \quad (43)$$

where T_c is the period of the thermal cycle.

Thermal fatigue can also lead to bonding layer failure, while corrosion contributes to bonding wire failure. The *TTF* for bonding layer and bonding wire is denoted as TTF_{BL} and TTF_{BW}, respectively. Ultimately, competing failure rule is applied to the failure of all the sites. The time-to-failure of the device can be obtained by

$$TTF_D = \min(TTF_{DIE}, TTF_{BL}, TTF_{BW}, TTF_{SJ}). \quad (44)$$

TTF corresponding to the failure mechanism can be calculated by failure mechanism models listed in TABLE 1. And the values of model parameters are listed in TABLE 9.

The parameters in the failure mechanism models are assumed to obey the triangle distribution, the feature parameters of which are shown in TABLE 9. With the distribution assumptions and parameter sampling ($N = 10000$), the TTFs of multi failure mechanisms in different device sites can be calculated individually by the failure mechanisms models, shown in FIGURE 8 (a)-(h).

TTFs of Multi-mechanism failure can be obtained by cumulative damage theory and competing failure theory for different sites in this device. For die site, four failure mechanisms, including TDDB, HCI, SM, and EM, accord with competing failure theory. For solder joints, vibration fatigue and thermal fatigue can be accumulated together based on the cumulative damage. For the multi-site failure in this device, the competing failure theory can be utilized to determine the fatal failure mechanism and evaluate the device's lifetime.

TABLE 9. Values of model parameters and feature parameters of distribution.

Sites	Models	Parameters	Parameter $\boldsymbol{S}$, $\boldsymbol{\Theta}$ and distributions Lower limit a	Upper limit b	Mode c	Other parameters		Ref.
Die	TDDB	T	313	343	328	a_t	0.123	[35]
		E_{ox}	6.81	6.99	6.90	E_{at}	1.98	
		A_t	3.73e-11	9.73e-11	6.73e-11			
	HCI	T	313	343	328	N_h	3	
		I_{sub}	1.55e-6	2.15e-6	1.85e-6	E_{ah}	0.11	
		A_h	2.2e-8	4.0e-8	3.1e-8			
	EM	T	313	343	328	J_{crit}	2e4	
		J	1.95e5	2.55e5	2.25e5	N_e	2	[25]
		A_e	4.27e6	4.87e6	4.57e6	E_{ae}	0.84	
	SM	T	313	343	328	T_0	505	
						N_s	2.33	[27]
		A_s	2.3e8	2.9e8	2.6e8	E_{as}	0.58	
Wire bond	Corrosion	T	313	343	328	a_c	3.5e-2	[28]
		RH	0	0.30	0.15	E_{ac}	1.1	
		A_c	5.6e-10	6.56e-9	3.56e-9			
Bonding layer	Thermal fatigue	ΔW	1.22	3.02	2.12	K_1	2.24e4	[36]
						K_2	-1.52	
		a_{tf}	0.024	0.036	0.030	K_3	5.86e-7	
						K_4	0.98	
Solder joint	Thermal fatigue	ΔW	0.35	0.65	0.5	K_1	2.24e4	[36]
						K_2	-1.52	
		a_{tf}	0.388	0.400	0.394	K_3	5.86e-7	
						K_4	0.98	
	Vibration fatigue	$\Delta\varepsilon_1$	5.262e-5	5.50e-5	5.382e-5	n	-8.3	[30]
		N_0	268	328	298			
		$\frac{E}{3.5\sigma_u}$	0.001950	0.002100	0.002025			

100, 000 samples of device failure datasets are analyzed, and the fatal failure mechanisms proportion are statically computed, shown in FIGURE 8 (i). The potential occurrence ratios of die TDDB, solder joint fatigue and bonding wire corrosion are individually counted as 81.6%, 18.2% and 0.2%. The die TDDB can be considered as the highest possible one of the main failure mechanisms for this device.

Based on PoF and multi-mechanism failure analysis, the distribution diagram of the fatal failure TTFs is shown in FIGURE 9 (a), which indicates a double-peak distribution feature. The reliability distribution diagram of the device is shown in FIGURE 9 (b).

Lognormal, Weibull and MaxEnt methods are applied to fit the multi-mechanism failure MC sampling data. As shown in FIGURE 9 (a), Lognormal distribution, Weibull distribution, and 3-order MaxEnt distribution can only express the single peak characteristic with poor fitting results. The peak value of Weibull distribution and 3-order MaxEnt distribution locate between two peaks of the TTF distribution. The peak value of Lognormal distribution appears near the left peak of the TTF distribution. MaxEnt distributions with 4 to 7 orders present the double modal feature with better fitting results. With the increase of the order number, the MaxEnt distribution is more descriptive for the sampling data.

The RMSEs and AICs of Lognormal, Weibull, and 3- to 7-order MaxEnt distribution are compared in FIGURE 10. The 7-order MaxEnt PDF possesses the lowest RMSE and AIC, which means the most accurate and efficient fitting of samples. From the 4-order and the higher orders, the MaxEnt has a lower RMSE and AIC compared with the other two methods, on account of the emergence of the double modal feature, as shown in FIGURE 9 (a). And there is a clear trend of decreasing RMSE and AIC with the increase of the order of MaxEnt PDF.

For the high order MaxEnt PDF represents the MC sampling data well, and a more accurate reliability evaluation can be made using a better-fitted distribution, the 7-order MaxEnt PDF was chosen for the reliability evaluation of the device. The reliability distribution (reliability versus time) is presented in FIGURE 9 (b). The average lifetime, the medium lifetime is 17667129.19 s and 14657915.20 s respectively, and the resulting 95% confidence interval is 2619487.48 s to 40276017.48 s. The results listed in TABLE 10 indicate that the MaxEnt method gives the most accurate estimates among the three distributions.

V. DISCUSSION

PoF technique is practical and efficient in the reliability evaluation and lifetime prediction of semiconductor devices. However, the existing studies failed to fit the failure data well, especially when faced with multi-point and multi-mechanism failure. Consequently, the reliability evaluation only based on PoF technique cannot describe the multi-mechanism failure. In this study, PoF models, MC sampling for multi-mechanism failure and MaxEnt PDF are presented. The PoF models are used to predict TTFs corresponding to the single

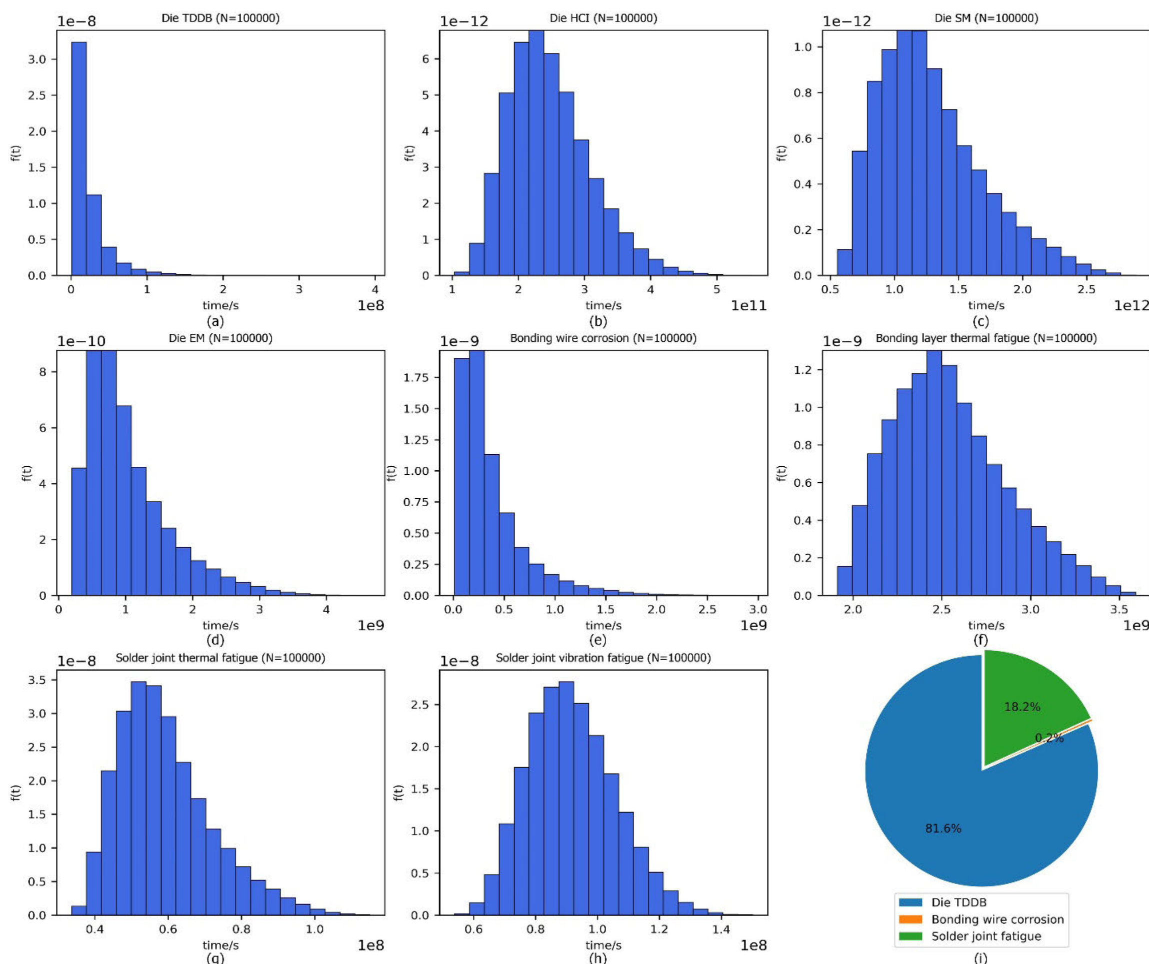

FIGURE 8. The TTF histograms of multi failure mechanisms and fatal failure mechanisms proportion pie chart.

TABLE 10. Lifetime predictions (Seconds) of MC sampling (N = 100000) by Lognormal method, Weibull method and MaxEnt method.

	Sampling data	Lognormal		Weibull		7-order MaxEnt	
		Estimate	Error	Estimate	Error	Estimate	Error
Average	**17667129.06**	18423908.57	4.3%	17702300.69	0.2%	17667129.19	0.0%
Medium	**14829226.46**	13733857.43	7.4%	15714141.42	6.0%	14657915.20	1.2%
Interval estimation	**(2701636.79,**	(3057172.61,	13.2%	(1962694.10,	27.4%	(2619487.48,	3.0%
($CL = 95\%$)	**40020917.07)**	61697150.81)	54.2%	44599572.97)	11.4%	40276017.48)	0.6%

failure mechanisms in every single point in the semiconductor devices. PoF models calculate TTFs by inputting loading conditions and structure and process-related parameters. Thus, a notable advantage of using PoF models is that the reliability evaluation can be conducted as early as the design stage. A mass of PoF models is included, which cover multiple potential failure mechanisms in semiconductor devices under operating conditions. For example, the thermal fatigue of the solder joints and the electromigration of the metal interconnects are proceeding simultaneously when the device is working. FIGURE 9 suggests that it is necessary to consider multiple failure mechanisms. The lifetime sampling data actually exhibits the double-peak characteristic, while the TTF sampling data of a single mechanism usually exhibits a single peak feature in FIGURE 8 (a)-(h). According to FIGURE 8 (i), the main failure mechanism in this case study is TDDB. And the ratio of solder joint fatigue shows the second potential failure mechanism, inducing the second failure peak.

The cumulative damage rules and the competing failure rules are adopted to deal with the multi-mechanism failure process. Based on these rules above, TTFs of each single

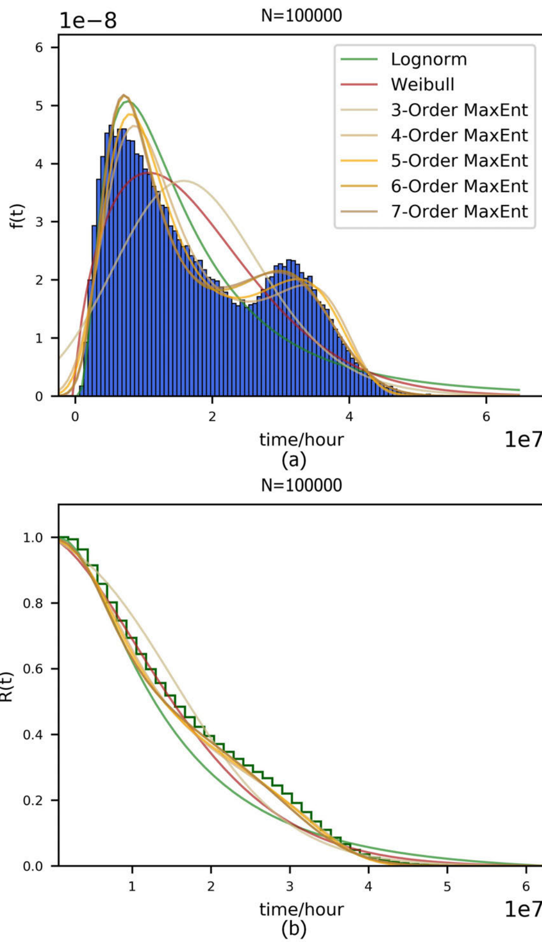

FIGURE 9. Estimated PDFs and reliability functions of multi-mechanism failure MC sampling ($N = 100000$) using Lognormal method, Weibull method and MaxEnt method with order numbers $n = 3$ to 7.

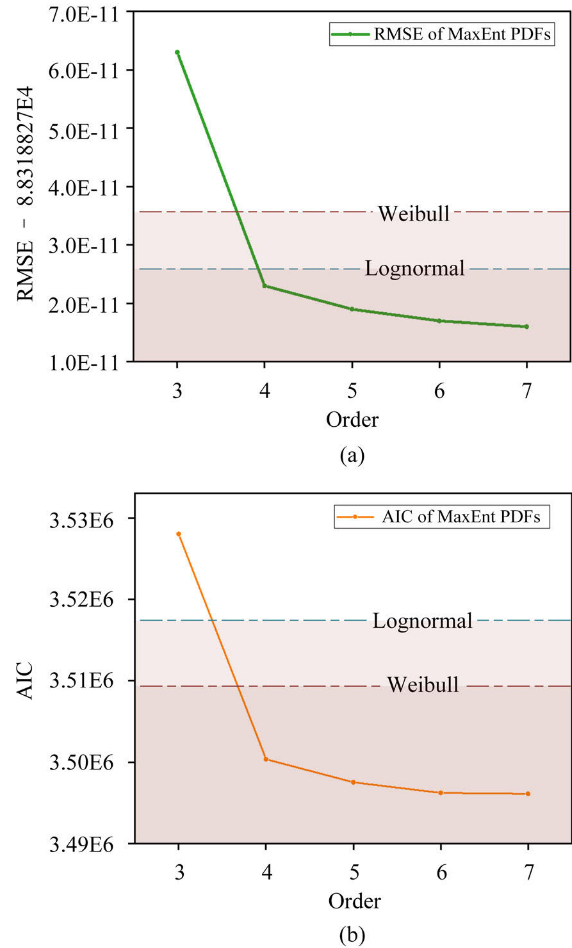

FIGURE 10. The RMSE and AIC of Lognormal method, Weibull method and MaxEnt method with order numbers $n = 3$ to 7 ($N = 100000$). RMSE has been normalized for presentation.

failure mechanisms can be used to predict the device lifetime of multi-mechanism failure. The cumulative damage rules are applied to calculate TTF of a failure point with multiple related mechanisms. For a typical semiconductor device in the case study, vibration fatigue and thermal fatigue of the solder joints are treated by the cumulative damage rules. Competing failure rules are used to deal with unrelated failure mechanisms at one single point or mechanisms of different points. Moreover, considering the fluctuation of loading conditions and the instability of the manufacturing processes, MC method is utilized to sample stochastic parameters of the specific distribution. Massive TTF data with sampled parameters based on PoF models are generated. By referring to the cumulative damage rules and the competing failure rules, the device lifetime sampling data are acquired. The histogram of the device lifetime is shown in FIGURE 9 (a).

The MaxEnt PDF fitting algorithm is proposed to fit the histogram of the lifetime sampling data. The reliability evaluation is performed based on the fitted PDF. The MaxEnt principle ensures that the data can be best represented by the MaxEnt PDF.

The MaxEnt principle states that the probability distribution which best matches the objective data has the largest entropy. Based on the thoughts, the MaxEnt PDF whose statistical characteristics of the random variable are most in line with the objective data is derived. Three numerical analysis examples are given to examine the goodness of fitting by Weibull, Lognormal, and MaxEnt PDFs. The results show that the high-order MaxEnt can fit well the sampling data of Weibull, Lognormal and bi-modal distributions, and the MaxEnt PDF has a significant advantage in processing the data with a bimodal feature, shown in FIGURE 6. The characteristics of the MaxEnt PDF are particularly suitable for processing the sampling data of the device failure. As shown in FIGURE 9 (b), the TTF histogram of the device exhibits a multi-modal feature under the effect of multiple-mechanism failure. Weibull for catastrophic failures and Lognormal for gradual wear out failures cannot fit the sampling data well in facing this situation, while the MaxEnt PDF can exploit its superiority to the full. The MaxEnt PDF makes the fewest assumptions about the true distribution of data and represents the data best. The fitting curves of the MaxEnt PDF in

FIGURE 9 (a) capture the sample data well. And more accurate reliability evaluations can be conducted using the MaxEnt PDF, shown in FIGURE 10 and TABLE 10. The physical meaning behind the fitted MaxEnt PDF is: the failure of the device is the result of multiple mechanisms, and the lifetime of the device is dominated by multiple mechanisms. A large number of failures will occur due to a certain mechanism at a certain time. The survived devices will continue to serve. And at a certain time after this time, another large number of failures will occur due to the leading role of another mechanism. Hence, the distribution of the device lifetime (i.e., the MaxEnt PDF) exhibits a multi-modal feature.

VI. CONCLUSION

In this study, we proposed an improved reliability evaluation approach for semiconductor devices with multi-mechanism failure based on PoF technique and MaxEnt principle. The PoF technique utilizes PoF model to calculate TTF corresponding to the failure mechanism, and MC sampling procedure, which considers the fluctuation of process and service conditions generate a batch of TTF sampling data. Cumulative damage rules and competing failure rules were used to deal with multi-point and multi-mechanism failure, and they work with MC sampling to generate lifetime sampling data of the device. The sampling data were fitted by MaxEnt PDF derived from the MaxEnt principle. And reliability evaluation was based on the fitted MaxEnt PDF. Three numerical analysis examples show that the MaxEnt PDF can fit most of the sampling data well. A case study was presented to explain the workflow of the proposed reliability evaluation approach. The lifetime sampling data of the device exhibits a double-peak characteristic because of the multiple failure mechanisms in the service conditions. And the MaxEnt PDF fits best and gives an accurate reliability evaluation.

This study focused on the MC sampling procedure of multi-mechanism failure and the MaxEnt principle-based sampling data processing. However, the complicated interactions between failure mechanisms, e.g., TDDB and HCI, are worth further research when an accurate lifetime prediction is required.

REFERENCES

[1] L. Klyatis, "Analysis of the current practices with reliability prediction," SAE Tech. Paper 2018-01-0100, Apr. 2018, doi: 10.4271/2018-01-0100.

[2] C. Hendricks, E. George, M. Osterman, and M. Pecht, "Physics-of-failure (PoF) methodology for electronic reliability," in *Reliability Characterisation of Electrical and Electronic Systems*. Amsterdam, The Netherlands: Elsevier, 2015, pp. 27–42.

[3] S.-J. Kim, T. Yuan, and S. J. Bae, "A spatio-temporal defect process model for competing progressive breakdown modes of ultra-thin gate oxides," *IEEE Trans. Rel.*, vol. 65, no. 1, pp. 263–271, Mar. 2016.

[4] G. Fu, Y. Su, W. Guo, B. Wan, Z. Zhang, and Y. Wang, "Life prediction methodology of system-in-package based on physics of failure," *Microelectron. Rel.*, vols. 88–90, pp. 173–178, Sep. 2018, doi: 10.1016/j.microrel.2018.06.119.

[5] W. Ahn, H. Zhang, T. Shen, C. Christiansen, P. Justison, S. Shin, and M. A. Alam, "A predictive model for IC self-heating based on effective medium and image charge theories and its implications for interconnect and transistor reliability," *IEEE Trans. Electron Devices*, vol. 64, no. 9, pp. 3555–3562, Sep. 2017, doi: 10.1109/TED.2017.2725742.

[6] H. Qi, M. Osterman, and M. Pecht, "A rapid life-prediction approach for PBGA solder joints under combined thermal cycling and vibration loading conditions," *IEEE Trans. Compon. Packag. Technol.*, vol. 32, no. 2, pp. 283–292, Jun. 2009.

[7] T. Eckert, M. Kruger, W. H. Muller, N. F. Nissen, and H. Reichl, "Investigation of the solder joint fatigue life in combined vibration and thermal cycling tests," in *Proc. 60th Electron. Compon. Technol. Conf. (ECTC)*, Jun. 2010, pp. 1209–1216.

[8] D. M. Fan, Y. Ren, Z. L. Wang, and L. L. Liu, "Mission reliability prediction methods for board level electronic equipment based on physics of failure and Bayesian networks," in *Proc. 1st Int. Conf. Rel. Syst. Eng. ICRSE)*. New York, NY, USA, Oct. 2015, pp. 1–7.

[9] J. Xu, L. Wang, Y. Li, Z. Zhang, G. Wang, and C. Hong, "A unified MMC reliability evaluation based on physics-of-failure and SM lifetime correlation," *Int. J. Electr. Power Energy Syst.*, vol. 106, pp. 158–168, Mar. 2019.

[10] J. Jiao, X. De, Z. Chen, and T. Zhao, "Integrated circuit failure analysis and reliability prediction based on physics of failure," *Eng. Failure Anal.*, vol. 104, pp. 714–726, Oct. 2019.

[11] W. Qiu, G. Lian, M. Xue, and K. Huang, "Physics of failure-based failure mode, effects, and criticality analysis for integrated circuits," *Syst. Eng.*, vol. 21, no. 6, pp. 511–519, Nov. 2018, doi: 10.1002/sys.21451.

[12] K. C. Kapur and M. Pecht, *Reliability Engineering*. Hoboken, NJ, USA: Wiley, 2014.

[13] E. T. Jaynes, "Information theory and statistical mechanics," *Phys. Rev.*, vol. 106, no. 4, pp. 620–630, May 1957, doi: 10.1103/PhysRev.106.620.

[14] H. Gotovac and B. Gotovac, "Maximum entropy algorithm with inexact upper entropy bound based on fup basis functions with compact support," *J. Comput. Phys.*, vol. 228, no. 24, pp. 9079–9091, Dec. 2009, doi: 10.1016/j.jcp.2009.09.011.

[15] M. Bee, "A maximum entropy approach to loss distribution analysis," *Entropy*, vol. 15, no. 3, pp. 1100–1117, Mar. 2013.

[16] B. Barzdajn, "Maximum entropy distribution under moments and quantiles constraints," *Measurement*, vol. 57, pp. 102–107, Nov. 2014, doi: 10.1016/j.measurement.2014.07.012.

[17] H. Dai, H. Zhang, and W. Wang, "A new maximum entropy-based importance sampling for reliability analysis," *Struct. Saf.*, vol. 63, pp. 71–80, Nov. 2016, doi: 10.1016/j.strusafe.2016.08.001.

[18] X. Zhang, J. Liu, Y. Yan, and M. Pandey, "An effective approach for reliability-based sensitivity analysis with the principle of maximum entropy and fractional moments," *Entropy*, vol. 21, no. 7, p. 649, Jul. 2019.

[19] F. Xiong, S. Guo, L. Chen, J. Yin, and P. Liu, "Flood frequency analysis using halphen distribution and maximum entropy," *J. Hydrologic Eng.*, vol. 23, no. 5, May 2018, Art. no. 04018012.

[20] A. Rajan, Y. Chow Kuang, M. Po-Leen Ooi, and S. N. Demidenko, "Moments and maximum entropy method for expanded uncertainty estimation in measurements," in *Proc. IEEE Int. Instrum. Meas. Technol. Conf. (I2MTC)*, May 2017, pp. 1–6, doi: 10.1109/I2MTC.2017.7969851.

[21] E. S. Anolick and G. R. Nelson, "Low-field time-dependent dielectric integrity," *IEEE Trans. Rel.*, vols. R–29, no. 3, pp. 217–221, Aug. 1980.

[22] D. L. Crook, "Method of determining reliability screens for time dependent dielectric breakdown," in *Proc. 17th Int. Rel. Phys. Symp.*, Apr. 1979, pp. 1–7.

[23] A. Berman, "Time-zero dielectric reliability test by a ramp method," in *Proc. 19th Int. Rel. Phys. Symp.*, Apr. 1981, pp. 204–209.

[24] *Failure Mechanisms and Models for Semiconductor Devices*, JEDEC, Richmond, VA, USA, 2016.

[25] J. R. Black, "Electromigration failure modes in aluminum metallization for semiconductor devices," *Proc. IEEE*, vol. 57, no. 9, pp. 1587–1594, Sep. 1969.

[26] J. T. Yue, W. P. Funsten, and R. V. Taylor, "Stress induced voids in aluminum interconnects during IC processing," in *Proc. 23rd Int. Rel. Phys. Symp.*, Mar. 1985, pp. 126–137, doi: 10.1109/IRPS.1985.362087.

[27] J. McPherson and C. Dunn, "A model for stress-induced metal notching and voiding in very large-scale-integrated Al-Si (1%) metallization," *J. Vac. Sci. Technol. B, Microelectron. Process. Phenomena*, vol. 5, no. 5, pp. 1321–1325, 1987.

[28] R. Rongen, G. M. O'Halloran, A. Mavinkurve, L. Goumans, and M.-L. Farrugia, "Lifetime prediction of cu-al wire bonded contacts for different mould compounds," in *Proc. IEEE 64th Electron. Compon. Technol. Conf. (ECTC)*, May 2014, pp. 411–418.

[29] R. Darveaux, "Effect of simulation methodology on solder joint crack growth correlation," in *Proc. 50th Electron. Compon. Technol. Conf.*, May 2000, pp. 1048–1058.

[30] D. S. Steinberg, *Vibration Analysis for Electronic Equipment*. New York, NY, USA: Wiley, 1988.

[31] D. Barker, J. Vodzak, A. Dasgupta, and M. Pecht, "Combined vibrational and thermal solder joint fatigue—A generalized strain versus life approach," *J. Electron. Packag.*, vol. 112, no. 2, pp. 129–134, 1990, doi: 10.1115/1.2904353.

[32] C. E. Shannon, "A mathematical theory of communication," *Bell Syst. Tech. J.*, vol. 27, no. 3, pp. 379–423, Jul. 1948, doi: 10.1002/j.1538-7305.1948.tb01338.x.

[33] F. Louzada, P. L. Ramos, and D. Nascimento, "The inverse Nakagami-m distribution: A novel approach in reliability," *IEEE Trans. Rel.*, vol. 67, no. 3, pp. 1030–1042, Sep. 2018.

[34] Z. Xi, C. Hu, and B. D. Youn, "A comparative study of probability estimation methods for reliability analysis," *Struct. Multidisciplinary Optim.*, vol. 45, no. 1, pp. 33–52, Jan. 2012.

[35] A. M. Yassine, H. E. Nariman, M. McBride, M. Uzer, and K. R. Olasupo, "Time dependent breakdown of ultrathin gate oxide," *IEEE Trans. Electron Devices*, vol. 47, no. 7, pp. 1416–1420, Jul. 2000.

[36] J. H. L. Pang, D. Y. R. Chong, and T. H. Low, "Thermal cycling analysis of flip-chip solder joint reliability," *IEEE Trans. Compon. Packag. Technol.*, vol. 24, no. 4, pp. 705–712, 2001.

BO WAN (Member, IEEE) received the B.S. degree in mathematics and the M.S. and Ph.D. degrees in systems engineering from Beihang University, Beijing, in 2005, 2008, and 2017, respectively.

He is currently a Lecturer with the Institute of Reliability Engineering, Beihang University. His research interests include reliability simulation, reliability evaluation for electronics, and failure analysis.

YE WANG was born in Anhui, China, in 1996. He received the B.S. degree in quality and reliability of aircraft from the Institute of Reliability Engineering, Beihang University, Beijing, China, in 2017, where he is currently pursuing the Ph.D. degree in systems engineering.

His research interests include reliability analysis for manufacturing process, simulation of solder joint fatigue, and reliability evaluation for electronic systems.

YUTAI SU was born in Baotou, Nei Mongol, China, in 1991. He received the B.S. degree in quality and reliability engineering from Beihang University, Beijing, China, in 2013, where he is currently pursuing the Ph.D. degree in systems engineering.

From 2018 to 2019, he was a Visiting Researcher with the Wolfson School of Mechanical, Electrical and Manufacturing Engineering, Loughborough University, Loughborough, U.K. His research interests include reliability assessment of microelectronics, physics of failure theory, and multi-physics fields modeling of system-in-package.

GUICUI FU (Member, IEEE) received the B.S. degree in mechanical manufacturing technology and design from Shenyang Aerospace University, Shenyang, China, in 1990, the M.S. degree in flight vehicle design from Northwestern Polytechnical University, Xi'an, China, in 1993, and the Ph.D. degree in flight vehicle design from Beihang University, Beijing, China, in 2005.

She is currently a Professor of Systems Engineering with Beihang University, where she is also the Deputy Director of the Research Center for Component Quality Engineering. Her research interests include electrical devices qualification assurance, engineering failure analysis, manufacturing process reliability, and physics of failure theories.